Article type: Article

Title:

High Performance Anion Exchange Membrane Electrolysis using Plasma-Sprayed, Non-Precious Metal Electrodes

Li Wang[a,*], Thomas Weissbach[b], Regine Reissner[a], Asif Ansar[a], Aldo S. Gago[a], Steven Holdcroft[b] and K. Andreas Friedrich[a,c,*]

[a] Institute of Engineering Thermodynamics, German Aerospace Center (DLR), Pfaffenwaldring 38-40, 70569 Stuttgart, Germany
[b] Department of Chemistry, Simon Fraser University, 8888 University Drive, Burnaby, BC V5A 1S6, Canada
[c] Institute of Building Energetics, Thermal Engineering and Energy Storage (IGTE), University of Stuttgart, Pfaffenwaldring 31, 70569 Stuttgart, Germany

Corresponding authors: li.wang@dlr.de; andreas.friedrich@dlr.de

Key words: water electrolysis; anion exchange membrane; plasma-sprayed electrode; non-precious metal; green hydrogen production

Abstract:

The production of green hydrogen by a cost-effective electrolysis technology is of paramount importance for future energy supply systems. In this regard, proton exchange membrane (PEM) electrolysis is the technology of choice due to its compactness and high efficiency, however its dependence on the scarce iridium catalyst jeopardizes the deployment at large scale. Here, we present a low cost electrolyzer consisting of an assembly of an anion exchange membrane (AEM) and plasma-sprayed electrodes without any precious metals. Several electrode materials are developed and tested in this configuration at 60 °C and feeding 1M KOH electrolyte. The AEM electrolyzer with NiAlMo electrodes is able to achieve a potential of 2.086 V at a current density of 2 A cm^{-2}, which is comparable to the performances of industrial MW-size PEM electrolyzers. The cell potential with NiAl anode and NiAlMo cathode is 0.4 V higher at the same current density, but it keeps a stable operation for more than 150 h. Through different post-mortem analyses on the aged electrodes, the degradation mechanism of NiAlMo anode is elucidated. The efficiencies of the developed AEM electrolyzer concept reported herein are close to those of the commercial PEM systems, and thus a cost-effective alternative to this technology is provided based on our results.

Introduction:

Climate change that is caused by the anthropogenic activities leading to higher CO_2 concentrations – 405 ppm in 2017 compared to 295 ppm in 1900 – in the atmosphere is becoming more apparent recently and is one of the major challenges for society.[1] Therefore carbon-neutral energy systems are being developed to mitigate this effect, in which the electricity is produced from renewables and green hydrogen is produced for transport, industry and power. As one of the dominating electrolysis techniques, low temperature water electrolysis consists either of the mature and established traditional alkaline water electrolysis (AEL) or the more advanced proton exchange membrane (PEM) electrolysis. In the last decade, anion exchange membrane (AEM) electrolyzers have been demonstrated that may combine advantages of AEL (low cost materials) and PEM (high performance). The first one is technologically mature and used in industry for many decades, made of two Ni-based electrodes that are separated by a diaphragm, however its performance is limited by restrictions and disadvantages including low current density and small operation range and highly concentrated KOH (normally 6M) which needs to be circulated.[2,3] Comparatively, PEM electrolyzers overcome most of these restrictions, being a versatile player with the advantages of compact system design, fast response, dynamic operation and excellent overload capacity and high voltage efficiency.[4] But the high capital expenditure (CAPEX) investment hinders it from the large-scale deployment, which is mainly contributed by the titanium bi-polar plates and catalyst coated membranes (CCM) that contains platinum group materials.[5,6] Moreover, the scarcity of iridium – the only technically feasible anode catalyst for PEM electrolzyers – in our planet further impedes it from TW-scale production in the long run.[7] In recent years, AEM electrolyzers are emerging as a relatively new technique owing to the rapid advances of the component materials, especially the anion exchange membrane (AEM) which was a critical point in the past in terms of ion exchange capacity and stability.[8] The advantage of the AEM electrolyzers includes: 1) they have all the merits of PEM

electrolyzers, but can eliminate expensive precious metal group electrocatalysts and titanium components that in future may account for more than 50 % cost of PEM systems;[4–6] 2) they do not require the high concentration KOH electrolyte as feedstock unlike traditional AEL, both deionized water and low concentration KOH/other types salts are possibilities which are less corrosive and operator-friendly and a prerequisite for stable organic membranes;[8–10] 3) depending on the membrane AEM may enable the pressurization of only the hydrogen side therefore becoming more efficient from the system point of view.

The first key beneficial aspect of AEM electrolyzers is the electrodes without precious metals, including both cathode and anode which promote the hydrogen evolution reaction (HER) and oxygen evolution reaction (OER), respectively. Non-precious metal based nanoparticles, such as Ni,[11,12] NiMo[13,14] and NiP,[15,16] are commonly employed as cathode catalysts while NiFe oxyhydroxide,[17] $NiFe_2O_4$,[18] $CuCoO_x$[19,20] and Ni/CeO_2-La_2O_3/C[8] are those frequently used for the anode. In some studies, even precious metal catalyst Pt/C and IrO_x/IrO_2 are used as cathode and anode catalyst respectively to achieve a high cell performance.[10,21,22] Both catalyst coated membrane (CCM) and catalyst coated substrate (CCS) techniques by different coating methods including wet spray, dry spray, doctor blade, screen printing and ultrasonic spray,[23–25] which are the standard electrode processing techniques for PEM fuel cells and PEM electrolyzers, are the primary approaches of electrode preparation for AEM electrolyzers.[26] Liu et al. deposited NiFeCo nanoparticles on carbon paper as the cathode and $NiFe_2O_4$ particles on a sintered stainless steel fiber felt as the anode, a cell voltage of 1.9 V at the current density of 1 A cm^{-2} was achieved at 60 °C.[18] Ito et al. reported that the electrodes prepared by CCM approach for AEM electrolyzers has a higher efficient mass transport of ions than CCS method.[26]

Another key aspect of AEM electrolyzers is the AEM. The membrane plays an essential role on the cell performance in terms of its ion conductivity, chemical stability, as well as the

mechanical stability and dimensional stability. Tokuyama A201 (Tokuyama Corp., Japan), Fumatech FAA-series (Fumatech Corp., Germany) and Sustainion membrane (Dioxide Material Corp., USA) are the most tested membranes in this field.[8,9,18,26] Several strategies have recently been explored with a view to increasing the alkaline stability of cationic polymers,[27–32] including dialkylated poly(benzimidazolium)s that possess steric hindrance around the C2-position of the benzimidazolium ring, in order to retard the rate of hydroxide ion attack.[33,34] The latter are stable for extended periods in 1 M hydroxide solution at 80 °C.[35]

In this work, a new concept of AEM electrolyzer with a number of beneficial properties is presented, a recently developed AEM, 2,2'',4,4'',6,6''-hexamethyl-*p*-terphenylene polydimethylbenzimidazolium (HTM-PMBI)[35] is used as electrolyte and non-precious metal electrodes fabricated by direct current (d.c.) plasma spraying on gradient porous metal framework (GPMF) are employed as anode and cathode, respectively. Electrode package made by plasma spraying on GPMF as a complete unit is unique and new in this study. In d.c. plasma spraying, finely divided surfacing materials such as powders are heated and accelerated in a plasma jet, which is formed by ionizing gaseous mixture by an electric arc. The powder particles form deposits on a prepared substrate due to their impingement, flattening into splats, rapid solidification, layering and consolidation (see Figure 1 (a)).[36] The deposits produced by plasma spraying are typically 10 μm to 1 mm in thickness and the deposition rates are in the range of 150 – 250 μm h^{-1} m^{-2}, significantly higher than the vapour based methods (chemical vapour deposition, physical vapour deposition, sputtering), plating processes and most of the printing techniques. As the deposits are produced from dry powder, plasma spraying enables to avoid development and costs of inks, slurry, targets, and organic precursors, and the consolidation of the particles can occur without a binder. Mechanical and functional properties of deposits are therefore dependent on inter-particle cohesion and not on binder characteristics. Plasma spraying is best suited for inorganic materials which do not

decompose or transform at high temperatures. It is a random deposition process which makes the control of microstructure of deposits challenging (see Figure 1 (b)).

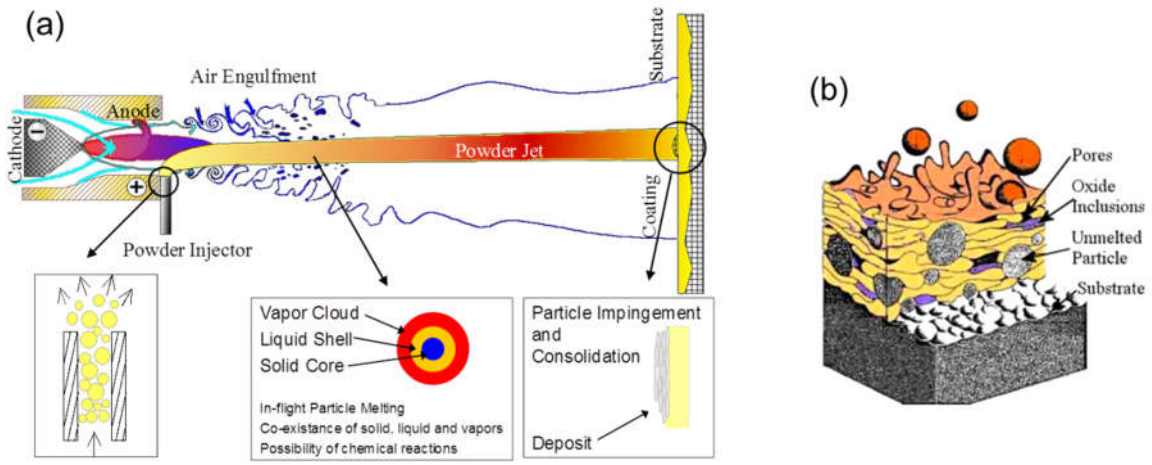

Figure 1. Schematic diagram of plasma spraying (a) and a resulting deposit with complex structure (b).[36]

The German Aerospace Center (DLR) has improved traditional alkaline water electrolysis efficiency by plasma spray coating of electrode sheets since the 1980s.[37] By using nickel sheet electrodes coated with NiAlMo (cathode) and NiAl (anode) by vacuum plasma spraying (VPS) or atmospheric plasma spraying (APS) an overpotential reduction of more than 250 mV as compared to the uncoated nickel electrode can be achieved.[38] By activation the coating layers are converted into Raney-nickel with a very high specific surface area. With additions of oxides to the anode further improvements could be obtained. Herein, we introduce the same approach including both VPS and APS to prepare the electrodes on GPMF for AEM electrolyzer application in the above-mentioned novel configuration. Four electrode compositions were prepared in this study: NiAlMo, Ni/Graphite, pure Ni and NiAl, of which NiAlMo is used for both cathode and anode while the others are only used for anode. NiAlMo, pure Ni and NiAl have been reported in the past by our group for conventional alkaline electrolyzers but NiAlMo had never been tested as anode,[38] Ni/Graphite is newly developed exclusively for this purpose. The assembled cells were tested under different conditions. The

one using NiAlMo anode achieved a cell voltage of 2.086 V with 2 A cm^{-2} at 60 ^{o}C when 1M KOH is used as feedstock, which is close to the current commercially available PEM electrolyzers – 2 V with 2 A cm^{-2}.[39,40] 154 hours stability was demonstrated for NiAl anode due to our testing time and much longer stabilities are probable. Under the operation conditions, electrochemical impedance spectroscopy (EIS) is conducted and used for the analysis of cell characteristics. Metallography, scanning electron microscopy (SEM), energy-dispersive X-ray spectroscopy (EDX) and element mapping are applied to the freshly-activated electrode and aged samples and the degradation mechanism of NiAlMo anode is elucidated.

Experimental section:

1, Membrane preparation

Hexamethyl-*p*-terphenyl poly(benzimidazolium) solid polymer electrolyte (HMT-PBI) was synthesized as described previously.[35] HMT-PMBI possessed 89% degree of methylation, which translates to an IEC of 2.52 mmol/g in the OH^- form.

HMT-PMBI was dissolved in DMSO by stirring and gently heating. The polymer solution was vacuum filtered through glass fibre at room temperature, cast on a levelled glass plate using a K202 Control Coater casting table and a doctor blade (RK PrintCoat Instruments Ltd) and dried in an oven at 85 °C. After soaking the membrane in distilled water for 24 h, the membrane was dried under vacuum at 80 °C for 24 h.

2, Fabrication of plasma sprayed electrode package

For the fabrication of the electrode package, powders of pure Ni, Ni-cladded-graphite, NiAl or NiAlMo were sprayed on the dense layer of the stainless steel gradient porous metal framework (GPMF, 4.25 mm thickness and 1.199 ± 0.002 g cm^{-2} area specific weight, MeliCon GmbH, Germany) by two different methods: atmospheric plasma spraying (APS) or

vacuum plasma spraying (VPS). APS was performed with Triplex-Pro210 plasma gun from Oerlikon-Metco (CH), whereas VPS was done using a F6 gun with Mach 3 deLaval nozzle from Medicoat (CH). The guns used in the current are shown in Figure 2. The primary plasma forming gas for both processes was Ar in which H_2 and/or He are added as secondary gases. In both processes, the spray powder were injected through external injection nozzles into the plasma jet, where particles were accelerated and heated due to momentum and heat transfer between plasma and particles, and the quasi or fully molten particles impacted the substrate surface, flatten, solidify and consolidate to form coating. Multiple layers were coated to form electrodes of suitable thickness. The detailed information is given in Table 1. One has to note that plasma spraying process may result in some variation of the coating quality from batch to batch as its intrinsic feature, therefore carefully selecting the spraying parameters and operator's experience are needed to maximally mitigate this effect. As a very broad estimate of the fabrication cost, a 100 μm thick coating for such a nickel base electrodes by plasma spraying would vary between 40 to 120 € per m² in mass production.[41]

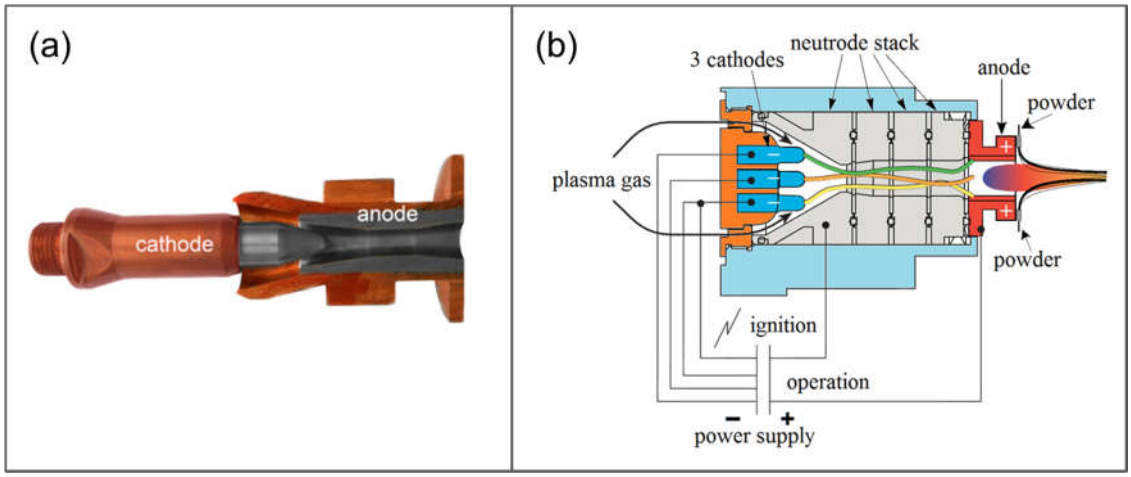

Figure 2. Two types of plasma spray guns used in this work: a single cathode single anode with deLaval contour F-6 type gun for VPS (a) and a three cathode cascaded anode Triplex Pro gun for APS (b).

Table 1. The detailed experimental parameters for plasma spraying.

Powder	Powder Supplier	Powder Composition	Particle Size$^{\Psi}$	Spray Process	Plasma net energy	Deposit thickness$^{\Psi}$	Deposit loading
Pure Ni	Praxair	99.95% Ni	35±5 μm	VPS	19 kW	91 ± 7 μm	78.9 mg cm^{-2}
Ni/Graphite	Praxair	Ni-25 wt.% C-balance	90 μm	APS	27 kW	107 ± 9 μm	57.7 mg cm^{-2}
NiAl	HC Stark	Ni-44 wt.% Al-balance	45±5 μm	APS	30 kW	87 ± 8 μm	47.9 mg cm^{-2}
NiAlMo	HC Stark	Ni-44 wt.% Al-19 wt.% Mo-balance	45±5 μm	APS	28 kW	88 ± 8 μm	42.7 mg cm^{-2}

$^{\Psi}$ Absolute deviation.

3, Concept

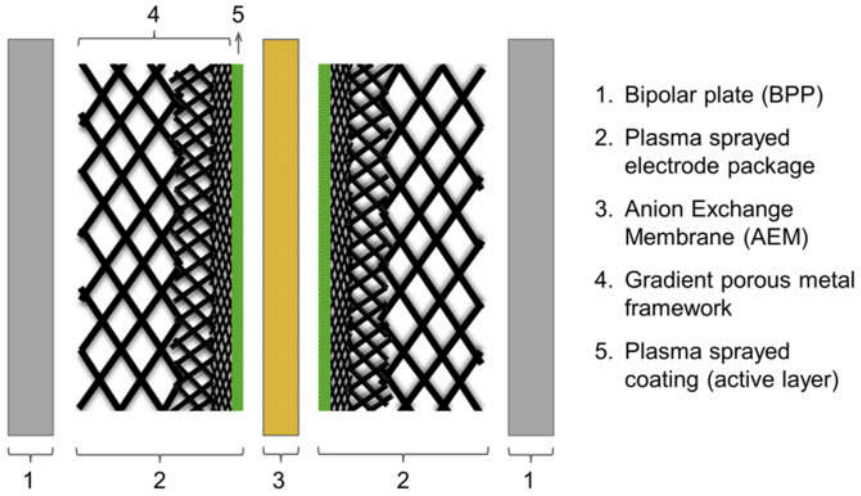

Figure 3. Schematic diagram of the AEM electrolyzer combining the plasma sprayed electrode package.

The schematic diagram of the newly developed AEM electrolyzer is shown in Figure 3, it consists of three main parts: bi-polar plates (1), plasma sprayed electrode package (2) and AEM (3). The core components are the plasma sprayed electrode package and the AEM, the former one (2) is composed of an active layer (5) that is prepared by plasma spray and a GPMF that provides the excellent mass transport for high current density operation owing to its gradient porous structure and adapted pore sizes. The cathode catalytic layer in this work is fixed as APS-sprayed NiAlMo due to its outstanding HER performance in alkaline

electrolyte.[42] APS-sprayed NiAlMo, APS-sprayed Ni/Graphite, VPS-sprayed Ni and APS-sprayed NiAl are taken as anode catalytic layer. All these layers were sprayed onto GPMF made of stainless steel no matter anode or cathode. The anion exchange membrane (3) ought to meet three criteria: i) high ion conductivity to ensure the high cell performance when using low concentrated KOH supporting electrolyte; ii) gas tightness to avoid the H_2/O_2 inter-crossover under high current density operation of the cell; iii) high chemical stability and mechanical/dimensional stability, which is the determining factor to the cell durability and complexities during the cell assembly. In this study, the AEM we used possesses 89% degree of methylation, which is equivalent to an ion exchange capacity (IEC) of 2.52 mmol/g in the OH^- form. The conductivity of the hydroxide ion form at 40 °C and 90% RH under constant current load has been previously reported to be 103 mS cm^{-1}.[43] The thickness of the membrane is 50 μm. In addition, both BPPs are also made of stainless steel. By implementing this concept, all the expensive components used in PEM electrolyzers are replaced by cost-effective materials but most of the advantages such as compact system, high current density and dynamic operation are retained.

4, AEM electrolyzer test

1) Electrode activation

The as-prepared electrodes were activated by using a typical procedure for removing aluminium from plasma sprayed coatings.[37] The electrodes were fully immersed in a mixed solution that contains 30 wt.% potassium hydroxide (KOH) and 10 wt.% potassium sodium tartrate tetrahydrate ($KNaC_4H_4O_6 \cdot 4H_2O$) and kept for 24 hours at 80 °C, afterwards transferred to DI water preventing from oxidation in air, ready for use.

2) Cell assembly and test

The electrolyzer cell used in this study has an active area of 4 cm^2 with the configuration shown in Figure 3. For the standard tests, stainless steel (SS) bi-polar plates (BPPs, 5 mm thickness, homemade) are used for both anode and cathode sides and 1M KOH solution is taken as feedstock unless specified. To assemble the cell, cathode BPP, tailored cathodic plasma sprayed electrode package, HMT-PMBI AEM (50 μm thickness), tailored anodic plasma sprayed electrode package and anode BPP are successively piled up and closed with SS bolts by using proper insulation. Once ready, pre-heated 1M KOH is fed to both anode and cathode, keep the circulation for 24 h to activate the HMT-PMBI membrane before operating the cell.

All the measurements were conducted by using a Zahner IM6ex Electrochemical Workstation coupled with an external potentiostat PP241 (ZAHNER-elektrik GmbH & Co. KG, Germany), the cell temperature is maintained at 60 °C during the tests. For each cell, the activity was measured before and after stability test, galvanostatic cycling between 0 A and 8 A with a ramp of 1 A min^{-1} were performed for three cycles for this purpose. The stability was evaluated by recording the cell voltage changes along with the operation time while a fixed current of 4 A was applied on the cell. Note that the different operation time for the stability tests was not caused by the system failure, but decided upon by the operator depending on the cell performance.

Electrochemical impedance spectroscopy (EIS) was conducted when the AEM electrolyzer was under operation with a constant current of 400 mA. A perturbation current (AC signal) with an amplitude of 50 mA in the frequency range from 100 KHz to 50 mHz was applied on the cell, simultaneously the impedance was recorded. EIS fitting was done by using the SIM function of THALES software (ZAHNER-elektrik).

To investigate the effect of different materials of BPP on the cell performance, pure Ni BPPs were also used for specific measurements when NiAlMo was used as anode. In this case, both anode and cathode SS BPPs were replaced by pure Ni BPPs while all other components and conditions kept the same. Additionally, this specific cell was also tested by using 1M $KHCO_3$ solution as feedstock at 60 °C.

5, Physical characterization

1) Metallographic analysis

The as-activated NiAlMo electrode, aged NiAlMo anode, Ni/Graphite anode, pure Ni anode and NiAl anode were cut in half to have the fresh cross-section exposed. EpoFix Resin (Struers) was used to fix and inlay the sample, followed by a polishing procedure to achieve a flat, mirror-like surface for analysis. The samples were analyzed by an Axioplan Universal Microscope (Zeiss).

2) Scanning electron microscopy (SEM), Energy dispersive X-ray spectroscopy (EDX) and element mapping

After metallographic analyses, all samples were taken for SEM analysis. A Zeiss Ultra Plus scanning electron microscope equipped with an XFlash 5010 detector (Energy Resolution: 123 eV at Mn Kα; Bruker Corp.) was employed for this purpose. Before analysis, carbon is coated on all the sample surface to enhance the electro-conductivity. The SEM images were recorded by using backscattered electron (BSE) signals, in order to highlight the element distribution with visual colour contrast. EDX was conducted to analyze the mass percentage of the elemental composition. Element mapping of the cross-section of those electrodes was done by performing EDX in spot mode.

Results and discussion:

1, Performance – activity and stability

First the pristine electrodes were activated following the procedure described in the former part to leach-out Al and form a highly porous catalytic layer with high active surface exposed to the reactant – H_2O/aqueous KOH. Taking the freshly-activated electrodes the cell is assembled according to the configuration shown in Figure 3, right afterwards 1M KOH electrolyte is fed to the cell in order to prevent the electrodes from oxidizing in air.

The assembled AEM electrolyzers were tested under different conditions at 60 °C. As shown in Figure 4 (a), current-potential (i-V) curves illustrate the initial performance of each cell using NiAlMo cathode and different anodes – Ni/Graphite, NiAl, pure Ni and NiAlMo – when 1M KOH electrolyte is taken as feedstock. The one with NiAlMo anode shows the highest performance among all four cells, achieved a cell potential of 2.086 V with a current density of 2 A cm^{-2}, which is close to the typical performance of PEM electrolyzer (2 V @ 2 A cm^{-2}) and far better than the other electrodes in this comparison. Through comparing with other works summarized in the literature,[8] the cell described in this study outperforms most of them. The cell using Ni/Graphite anode gives the lowest performance, 2.647 V for 2 A cm^{-2}. The initial performance of the cells using NiAl anode and pure Ni anode are equivalent while NiAl anode shows slightly better performance under low current density range and pure Ni anode is a little better at high current densities.

Durability is the most challenging requirement of electrolyzers, in particular AEM which still suffers from aging effects. In our study, which concentrated first on performance, the AEM electrolyzers were operated under 1 A cm^{-2} to evaluate their short-term stability except the cell with NiAlMo anode. Figure 4 (b) shows the cell voltage with NiAl anode for about 154 hours constant electrolysis under 1 A cm^{-2}, the horizontal curve illustrates the robustness of the cell components under such a high current density operation in 1M KOH at 60 °C. The cell performance (i-V curves) before and after stability tests are given in Figure S2(c) (see supporting information (SI)), showing an improved performance after stability test. It is

explained by the *in situ* formation of $Ni(OH)_2$/NiOOH layers on the Ni surface during electrolysis, which is a more active phase toward OER in base condition.[44] A similar phenomenon is also observed for the cell using pure Ni anode which is operated at 1 A cm^{-2} for 15 hours, the cell performance is enhanced after electrolysis operation (Figure S2(b), SI). In comparison, the cell using Ni/Graphite anode does not show any distinguishable improvement after electrolysis (Figure S2(a), SI) but is stable for 8 hours operation at 1 A cm^{-2}. The least stable cell is the one using NiAlMo anode, its high instability was observed among each cycles of the test between 0 A to 2 A cm^{-2}, which does not allow us to conduct a stability test under constant current density. The cell performance was measured with three cycles each day and repeated on different dates, the results are shown in Figure S1 (SI), suggesting a fast degradation of NiAlMo anode when operating the cell up to 2 A cm^{-2}.

Besides the standard test conditions above used, Ni metal plates are tested as BPPs in the cell with NiAlMo anode, and in addition 1M KOH and 1M $KHCO_3$ are used as supporting electrolyte, respectively. When 1M KOH is used as feedstock, the initial cell performance is competitive with SS BPP and becomes better after 3.5 hours electrolysis operation at 1 A cm^{-2}, shown in Figure S3 (SI). This can be explained by the additional active sites and activity which is formed in situ on the surface of Ni BPP in alkaline electrolyte enhancing both cathode (HER) and anode (OER) reactions.[44–46] Therefore with Ni BPP we have to consider two opposing effects, namely lower overpotentials for HER and OER with time and increased OER overpotentials due to the degradation of the NiAlMo active layer. As a consequence still an improved overall cell performance may be observed. When the feedstock is replaced by 1M $KHCO_3$, the cell voltage given in Figure 5 shows a sharp increase at the same current density than feeding 1M KOH. The performance loss is explained by two factors: i) the decreased ion conductivity in the AEM[35] due to build up of carbonates; ii) the lower catalytic activity of Ni-based catalysts in lower pH environment while 1M $KHCO_3$ delivers a pH value

of about 8 and 1M KOH is almost pH 14,[47] which is apparent by the relatively higher onset potential of the cell using 1M $KHCO_3$ feedstock than the one using 1M KOH feedstock, 1.425 V and 1.594 V, respectively.

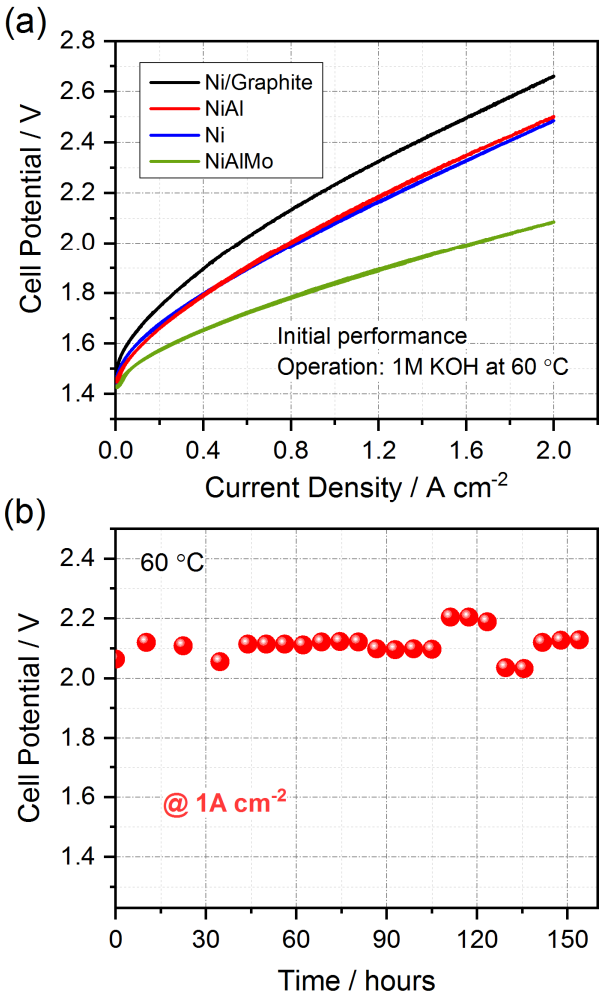

Figure 4. (a) AEM electrolyzer cell performance at 60 °C using NiAlMo cathode, HMT-PMBI AEM and different anodes: Ni/Graphite, NiAl, Ni and NiAlMo; (b) durability test of the cell using NiAl anode for about 154 hours under current density of 1 A cm^{-2}. SS BPPs are used in these tests.

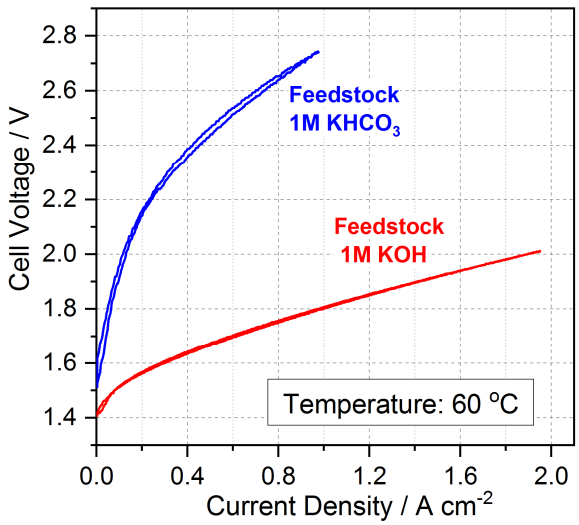

Figure 5. AEM electrolyzer cell performance comparison at 60 °C using 1 M $KHCO_3$ and 1 M KOH as feedstock, respectively; NiAlMo cathode, HMT-PMBI AEM, NiAlMo anode and Ni BPP are used in these tests.

2, EIS analysis

Electrochemical impedance spectroscopy (EIS) is a powerful tool that is commonly used for characterizing the PEM fuel cells and PEM electrolyzers.[48,49] Herein EIS is conducted on the AEM electrolyzer cell with NiAl anode for operation of 100 mA cm^{-2} and analyzed with a simple equivalent circuit to obtain an indication of resistance distribution of plasma sprayed electrodes in AEMs. The measured EIS spectrum is shown in Figure 6 and an equivalent circuit in the inset of Figure 6 is used for the fitting. The equivalent circuit is composed of an inductor, a resistor and four time constants in series while each time constant consists of a resistor and a constant phase element (CPE) in parallel. The inductor L represents the inductance of the connection cables; the resistor R represents the sum of the contributions from interfacial contact resistance between components and ohmic resistances of the cell components including AEM, plasma sprayed coating layer, GPMF and bipolar plates;[48] the four time constants successively represents the electrode surface roughness, cathodic charge transfer (HER), anodic charge transfer (OER) and mass transport processes (Figure S4, SI). It is worth to mention that: i) the rough internal surface is a typical feature of plasma sprayed electrode so that its effect has to be considered when building up the analysis model;[50] ii) the

kinetics of HER in alkaline electrolyte is much slower than in acid,[51] therefore the HER process has a significant contribution to the charge transfer resistance unlike in PEM electrolyzer, where this contribution is normally invisible in the EIS spectrum and is ignored. After fitting, R, R1, R2, R3 and R4 are separated with the value of 61.71 mΩ, 35.55 mΩ, 24.55 mΩ, 77.61 mΩ and 24.16 mΩ, respectively, which are listed in Table 2. It indicates the cell has an ohmic resistance of 61.71 mΩ and surface roughness of the electrodes contributes a resistance of 35.55 mΩ. The resistance of 24.55 mΩ and 77.61 mΩ are assigned to HER process on cathode and OER process on anode, respectively, which is consistent with the findings from literatures that HER in alkaline medium is a relatively slow process but still faster than OER.[37] It also indicates that the OER process is still one of the main barriers for AEM electrolyzer from achieving a high performance. The resistance of 24.16 mΩ is caused by the mass transport issues because plasma sprayed electrodes have a rather thick active layer which limits both water distribution and gas bubbles – H_2 and O_2 – detachment. The thickness will be adjusted in later experiments to find most suitable compromise between thickness and accessible active surface area.

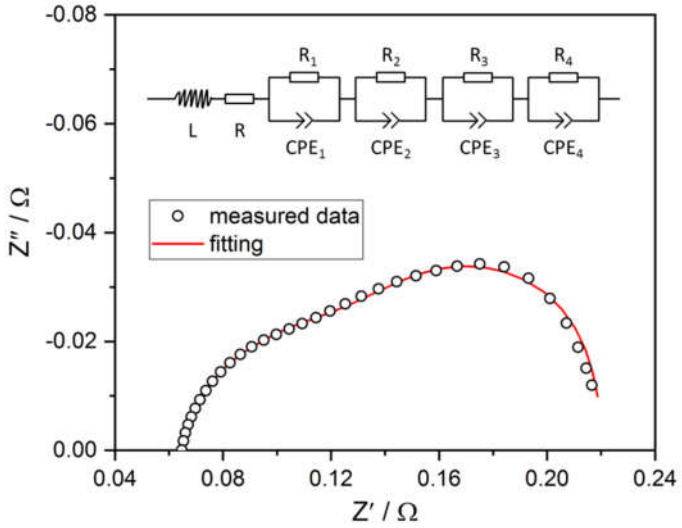

Figure 6. EIS analysis of the AEM electrolyzer cell using NiAlMo cathode, HMT-PMBI AEM and NiAl anode. The spectrum is recorded at 60 °C with the current density of 100 mA cm^{-2}.

Table 2. The resistance values derived from equivalent circuit (inset of Figure 6) fitting.

Circuit Elements	**R (mΩ)**	**R_1 (mΩ)**	**R_2 (mΩ)**	**R_3 (mΩ)**	**R_4 (mΩ)**
Resistance Value	61.71	35.55	24.55	77.61	24.16
Represented Processes	ohmic resistances (membrane and other components) + interfacial contact resistances	electrode surface roughness	cathodic charge transfer	anodic charge transfer	mass transport

3, Physical characterization of electrodes

In order to investigate the physical properties of these electrodes and especially the degradation mechanism of NiAlMo anode, the cross-section of one freshly-activated NiAlMo electrode and four aged electrodes after electrolysis operation – NiAlMo anode, Ni/Graphite anode, pure Ni anode and NiAl anode – were characterized by metallography, SEM, EDX and element mapping. Note that the operation time of the different electrodes vary from 8 to 154 hours. Figure 7 displays the cross-section of one freshly-activated NiAlMo electrode package, the plasma sprayed NiAlMo catalytic layer are mainly deposited on the top surface of the densest layer in the GPMF. Figure 8 shows the SEM images of all samples and element mapping in the corresponding analyzed area, the detailed mapping with individual elements are given in Figure S6 (SI). The SEM images are taken by using back scattered electrons (BSE) to enhance the colour contrast from different elements, the catalytic/active layer of all samples are clearly distinguished from the SS GPMF substrate with a uniform thickness between 65 μm and 75 μm. First, in Figure 8 (d-f, i) the freshly-activated NiAlMo electrode, aged NiAlMo anode and NiAl anode which were pre-treated in 30 wt.% KOH electrolyte to remove Al still show the residual Al in the catalytic layer with a number between 4.48 ± 0.36

wt.% and 9.38 ± 1.22 wt.% (see Table S1, SI), implying the pre-treatment procedure is not sufficient for removing all the Al in the electrodes. It can be speculated that it is especially Al in the closed pore that does not connect to the aqueous KOH which remains. Moreover, Al can also be bound with Ni in phases which prevent Al from leaching in a basic solution, for example Ni_3Al. Second, the freshly-activated NiAlMo electrode and aged NiAlMo anode do not show apparent difference in their main element composition, Ni is about 60 wt.%, Mo about 5 wt.% and O about 27 wt.%. The slight deviation is speculatively attributed to the heterogeneity of spraying process. Through comparing Figure 8 (a – f), the catalytic layer of aged NiAlMo anode is entirely detached from its SS GPMF substrate – active layer delamination (panel b, e and c, f in Figure 8) while it is not observed on the freshly-activated electrode (panel a and d in Figure 8). This is further confirmed by their metallographic analysis results shown in Figure S5 (a, b) (see SI), as we can see the dark active layer of freshly-activated NiAlMo electrode with a uniform thickness is tightly attached on the light colour SS GPMF substrate in Figure S5 (a) but the thickness of the aged one becomes uneven and a large crack clearly appears on the bottom position. The active layer delamination is correlated to the poor stability of NiAlMo anode in the test described in the former section and shown in Figure S1 (see SI). It is very likely that the Mo in the NiAlMo anode is present as a mixture component instead of solid solution alloy with Ni, so that Mo rapidly forms MoO_4^{2-} and dissolves in alkaline KOH solution whenever the potential is higher than 0.5 V vs. RHE,[52] resulting in crack formation in the active layer and eventually delamination. Moreover, the low adhesion force between NiAlMo layer and SS substrate accelerates this process at the interface.[53]

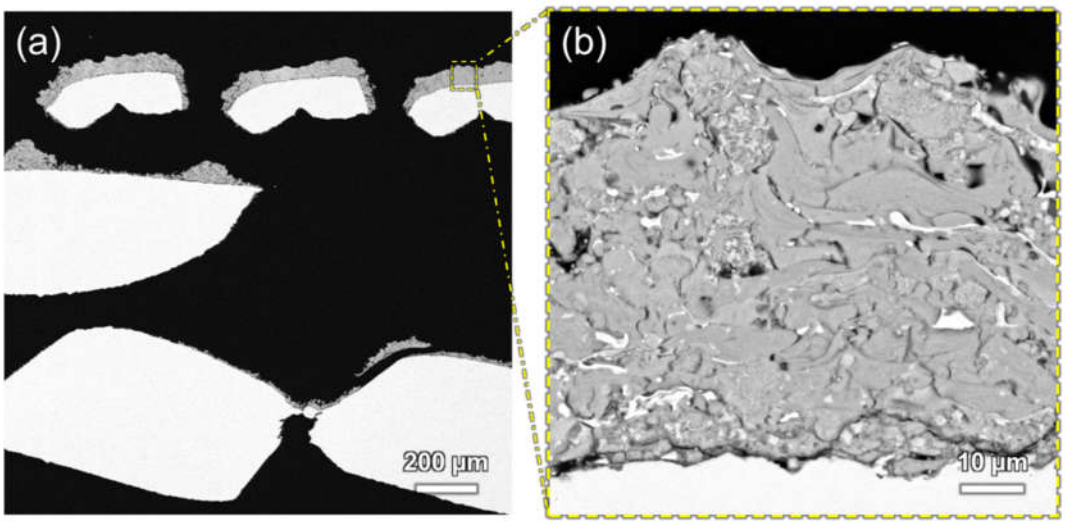

Figure 7. SEM images of one freshly-activated NiAlMo electrode with BSE signal: (a) overview of cross-section image of the typical electrode package (including the catalytic layer (grey colour) and the gradient porous metal framework (white colour) as current collector and mass transportation layer), black domains indicate the void space; (b) zoomed-in image of catalytic layer.

In Figure 8 (g, j), Ni/Graphite anode shows the greatest porosity visually among all the samples. However we have to consider that the sample surface was sputtered with carbon before SEM analysis for the sake of enhancing electro-conductivity. Therefore the C signal is not considered for the analysis. The black pores observed in the image of Ni/Graphite layer shown in Figure 8 (g) can be speculated to be graphite. In addition, metallographic image (Figure S5 (c), see SI) gives the complete picture of Ni/Graphite anode where graphite is clearly visualized inside the layer as dark and Ni as bright. Unlike what we expected, graphite was not removed from the active layer during electrolysis operation but rather remains inside the layer and blocks the water from accessing the Ni surface, which leads to the inferior AEM electrolyzer performance among all the samples shown in Figure 4 (a).

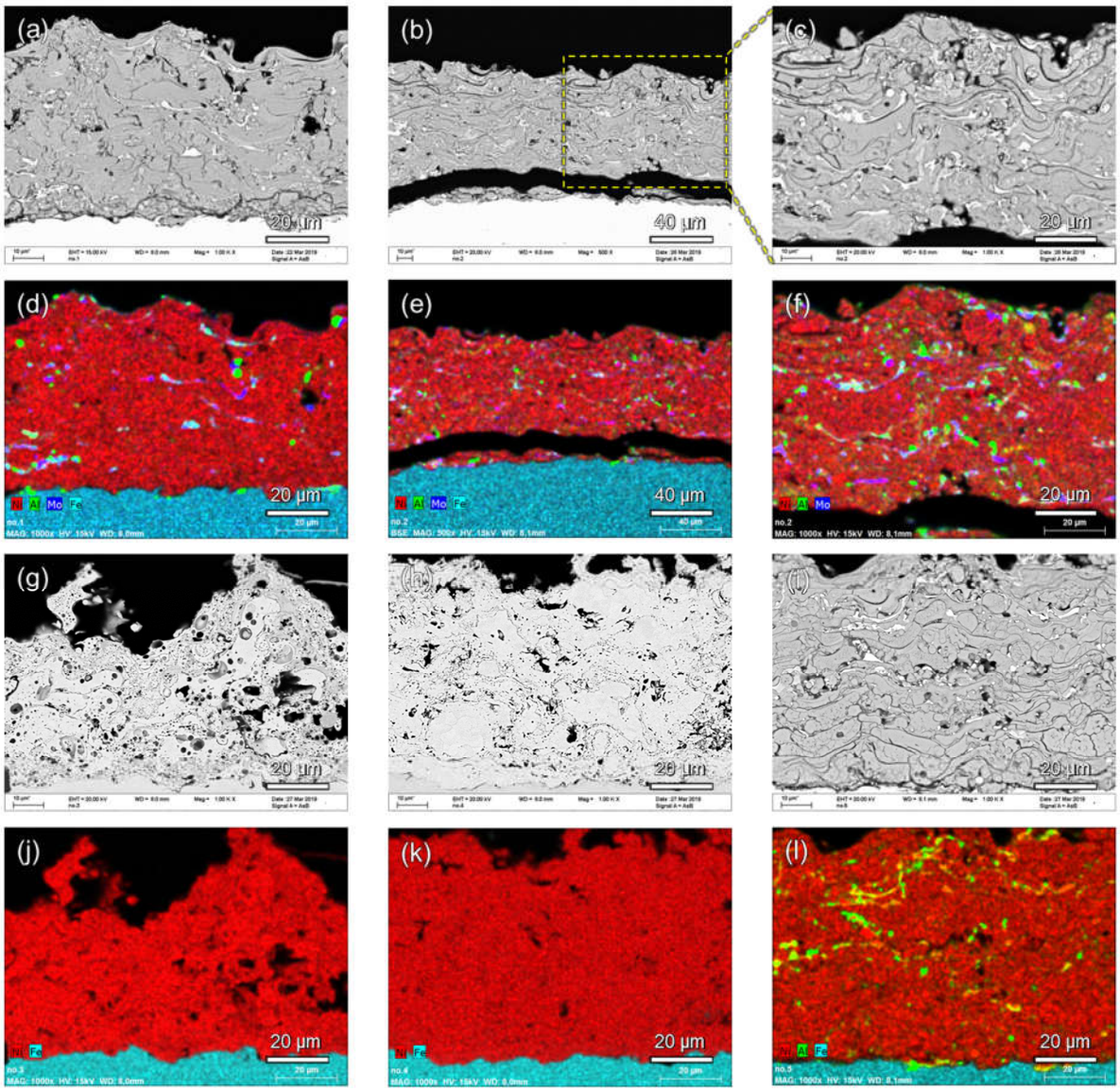

Figure 8. SEM images with back scattered signal (a-c, g-i) and their corresponding element mapping analysis (d-f, j-l): (a,d) freshly-activated NiAlMo electrode; (b, e and c, f) NiAlMo anode after operation up to 2 A cm^{-2}; (g, j) Ni/Graphite anode after 8 hours electrolysis; (h, k) pure Ni anode after 15 hours electrolysis; (i, l) NiAl anode after 154 hours electrolysis.

It is worth mentioning that O appears in all Al-containing electrodes with a ratio of about 27 wt.% while the Ni/Graphite anode and pure Ni anode have only 4.48 ± 1.28 wt.% and 2.29 ± 0.84 wt.%, respectively. This difference is attributed to two possible causes: i) Al has significantly higher affinity towards oxygen than pure Ni,[54] therefore the residual air/oxygen inside the plasma chamber are bound to precursor particles which then form oxides, leading to an increased O ratio in the coating layer; ii) electrode activation procedure, which is carried out in 30 wt.% aqueous KOH solution and applied to all Al-containing electrodes, promotes

the formation of NiO on the inner-surface of the coating layer so that O ratio increases. However oxygen-rich APS-sprayed NiAl anode compared to VPS-sprayed pure Ni anode does not show significant improvement in performance, suggesting that O proportion in the catalytic layer is not a crucial factor for manufacturing the highly performing plasma sprayed electrode.

Last but not least, the stability of AEM is another essential aspect to evaluate AEM electrolyzer, which is the critical property at present. Chemical stability ensures the high ion conductivity and therefore a constant cell performance. In this work the AEM electrolyzer with NiAl anode demonstrates about 154 hours stable operation at 60 ^{o}C with a current density of 1 A cm^{-2} in 1M KOH electrolyte. Figure 9 shows the digital photos of the AEM before and after operation for about 154 hours, the aged membrane shows 6.4 % expansion compared to its pristine state and no cracks and pin holes are observed, indicating both good mechanical and dimensional stability. In short, the newly developed AEM is a promising candidate for further advancing AEM electrolyzer technique, but much long-term test under dynamic operation and different conditions is needed in the future study.

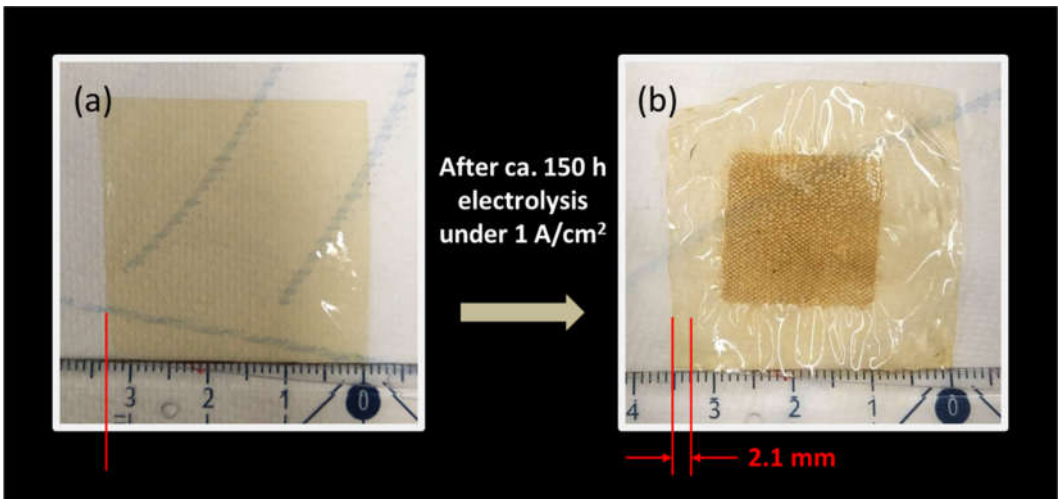

Figure 9. AEM dimensional changes after about 154 h electrolysis under 1 A cm^{-2}: (a) pristine AEM; (b) after about 154 h operation.

Conclusions:

In summary, we show a novel electrolyzer configuration that consists of an AEM compressed with two plasma sprayed electrode packages. A high performance that is comparable to PEM electrolyzer is achieved at 60 ^{o}C when APS-sprayed NiAlMo layer is used as anode and 1M KOH is supplied as feedstock. Comparatively, pure Ni, NiAl and Ni/Graphite are investigated as anode active layers and their short-term stability were evaluated, of which NiAl anode exhibited a stable behaviour during about 154 h operation with a current density of 1A cm^{-2}. Furthermore, different feedstocks (1M KOH and 1M $KHCO_3$) and different bi-polar plates (SS and pure Ni) are also tested and investigated. Even though there is still quite large room for different component materials to improve, e.g. the stability of NiAlMo anode, this newly developed AEM electrolyzer indicated the path to the cost-effective green hydrogen production.

Acknowledgement:

The authors thank Ina Plock (DLR Stuttgart) for her support on SEM analysis and Günter Roth (DLR Stuttgart) for the support on metallographic analysis; L. W. is grateful to Dr. Norbert Wagner (DLR Stuttgart) for the enlightening discussion of EIS analysis. S. H. thanks the Engineered Nickel Catalysts for Electrochemical Clean Energy Project supported by Grant No. RGPNM 477963-2015 under the Natural Sciences and Engineering Research Council of Canada (NSERC) Discovery Frontiers Program.

Supporting Information:

The Supporting Information is available free of charge on ACS Publications website. Membrane preparation, electrodes fabrication, electrochemical characterizations and additional SEM/EDX/Element mapping.

Notes

Poly(benz)imidazolium AEM technology is licensed by Simon Fraser University to Ionomr Innovations Inc., S. H. is a co-founder and minor shareholder of Ionomr Innovations Inc..

Reference:

(1) European Environment Agency. *Atmospheric Greenhouse Gas Concentrations.* Published on 20 March 2019. *https://www.eea.europa.eu/data-and-maps/indicators/atmospheric-greenhouse-gas-concentrations-6/assessment*

(2) Zeng, K.; Zhang, D. Recent Progress in Alkaline Water Electrolysis for Hydrogen Production and Applications. *Prog. Energy Combust. Sci.*, **2010**, 36, 307–326.

(3) Manabe, A; Kashiwase, M.; Hashimoto, T.; Hayashida, T.; Kato, A; Hirao, K.; Shimomura, I.; Nagashima, I. Basic Study of Alkaline Water Electrolysis. *Electrochim. Acta*, **2013**, 100, 249–256.

(4) Carmo, M.; Fritz, D. L.; Mergel, J.; Stolten, D. A Comprehensive Review on PEM Water Electrolysis. *Int. J. Hydrogen Energy*, **2013**, 38, 4901–4934.

(5) Bertuccioli, L.; Chan, A.; Hart, D.; Lehner, F.; Madden, B.; Standen, E. Study on Development of Water Electrolysis in the EU. *Final Report of Fuel Cells and Hydrogen Joint Undertaking*, **2014**, February.

(6) Mayyas, A.; Mann, M. Manufacturing Competitiveness - Analysis for Hydrogen Refueling Stations and Electrolyzers. *DOE Hydrogen and Fuel Cells Program*, **2018**, June.

(7) Paoli, E. A.; Masini, F.; Frydendal, R.; Deiana, D.; Schlaup, C.; Malizia, M;, Hansen, T. W.; Horch, S.; Stephens, I. E. L.; Chorkendorff, I. Oxygen Evolution on Well-Characterized Mass-Selected Ru and RuO_2 Nanoparticles. *Chem. Sci.*, **2015**, 6, 190–196.

(8) Vincent, I.; Bessarabov, D. Low Cost Hydrogen Production by Anion Exchange Membrane Electrolysis: A Review. *Renew. Sustain. Energy Rev.*, **2018**, 81, 1690–1704.

(9) Vincent, I.; Kruger, A.; Bessarabov, D. Development of Efficient Membrane Electrode Assembly for Low Cost Hydrogen Production by Anion Exchange Membrane Electrolysis. *Int. J. Hydrogen Energy*, **2017**, 42, 10752–10761.

(10) Fabbri, E.; Nachtegaal, M.; Binninger, T.; Cheng, X.; Kim, B. J.; Durst, J.; Bozza, F.; Graule, T.; Schäublin, R.; Wiles, L.; Pertoso, M.; Danilovic, N.; Ayers, K. E.; Schmidt, T. J. Dynamic Surface Self-Reconstruction is the Key of Highly Active Perovskite Nano-Electrocatalysts for Water Splitting. *Nat. Mater.*, **2017**, 16, 925–931.

(11) McArthur, M. A.; Jorge, L.; Coulombe, S.; Omanovic, S. Synthesis and Characterization of 3D Ni Nanoparticle/Carbon Nanotube Cathodes for Hydrogen Evolution in Alkaline Electrolyte. *J. Power Sources*, **2014**, 266, 365–373.

(12) Wang, T.; Zhou, Q.; Wang, X.; Zheng, J.; Li, X. MOF-Derived Surface Modified Ni Nanoparticles as An Efficient Catalyst for the Hydrogen Evolution Reaction. *J. Mater. Chem.*

A, **2015**, 3, 16435–16439.

(13) McKone, J. R.; Sadtler, B. F.; Werlang, C. A.; Lewis, N. S.; Gray, H. B. Ni-Mo Nanopowders for Efficient Electrochemical Hydrogen Evolution. *ACS Catal.*, **2013**, 3, 166–169.

(14) Wang, Y.; Zhang, G.; Xu, W.; Wan, P.; Lu, Z.; Li, Y.; Sun, X. A 3D Nanoporous Ni-Mo Electrocatalyst with Negligible Overpotential for Alkaline Hydrogen Evolution. *ChemElectroChem*, **2014**, 1, 1138–1144.

(15) Feng, L.; Vrubel, H.; Bensimon, M.; Hu, X. Easily-Prepared Dinickel Phosphide (Ni_2P) Nanoparticles as An Efficient and Robust Electrocatalyst for Hydrogen Evolution. *Phys. Chem. Chem. Phys.*, **2014**, 16, 5917–5921.

(16) Gong, M.; Wang, D. Y.; Chen, C. C.; Hwang, B. J.; Dai, H. A Mini Review on Nickel-Based Electrocatalysts for Alkaline Hydrogen Evolution Reaction. *Nano Res.*, 2016, **9**, 28–46.

(17) Dionigi, F.; Strasser, P. NiFe-Based (Oxy)hydroxide Catalysts for Oxygen Evolution Reaction in Non-Acidic Electrolytes. *Adv. Energy Mater.*, **2016**, 6, 1600621.

(18) Liu, Z.; Sajjad, S. D.; Gao, Y.; Yang, H.; Kaczur, J. J.; Masel, R. I. The Effect of Membrane on An Alkaline Water Electrolyzer. *Int. J. Hydrogen Energy*, **2017**, 42, 29661–29665.

(19) Wu, X.; Scott, K. $Cu_xCo_{3-x}O_4$ ($0 \leq x < 1$) Nanoparticles for Oxygen Evolution in High Performance Alkaline Exchange Membrane Water Electrolysers. *J. Mater. Chem.*, **2011**, 21, 12344–12351.

(20) Vincent, I.; Kruger, A.; Bessarabov, D. Hydrogen Production by Water Electrolysis with An Ultrathin Anion-Exchange Membrane (AEM). *Int. J. Electrochem. Sci.*, **2018**, 13, 11347–11358.

(21) Parrondo, J.; Arges, C. G.; Niedzwiecki, M.; Anderson, E. B.; Ayers, K. E.; Ramani, V. Degradation of Anion Exchange Membranes Used for Hydrogen Production by Ultrapure Water Electrolysis. *RSC Adv.*, **2014**, 4, 9875–9879.

(22) Park, E. J.; Capuano, C. B.; Ayers, K. E.; Bae, C. Chemically Durable Polymer Electrolytes for Solid-State Alkaline Water Electrolysis. *J. Power Sources*, **2018**, 375, 367–372.

(23) Hwang, D. S.; Park, C. H.; Yi, S. C.; Lee, Y. M. Optimal Catalyst Layer Structure of Polymer Electrolyte Membrane Fuel Cell. *Int. J. Hydrogen Energy*, **2011**, 36, 9876–9885.

(24) Mehta, V.; Cooper, J. S. Review and Analysis of PEM Fuel Cell Design and Manufacturing. *J. Power Sources*, **2003**, 114, 32–53.

(25) Park, I. S.; Li, W.; Manthiram, A. Fabrication of Catalyst-Coated Membrane-Electrode

Assemblies by Doctor Blade Method and Their Performance in Fuel Cells. *J. Power Sources*, **2010**, 195, 7078–7082.

(26) Ito, H.; Miyazaki, N.; Sugiyama, S.; Ishida, M.; Nakamura, Y.; Iwasaki, S.; Hasegawa, Y.; Nakano, A. Investigations on Electrode Configurations for Anion Exchange Membrane Electrolysis. *J. Appl. Electrochem.*, **2018**, 48, 305–316.

(27) Varcoe, J. R.; Atanassov, P.; Dekel, D. R.; Herring, A. M.; Hickner, M. A.; Kohl, P. A.; Kucernak, A. R.; Mustain, W. E.; Nijmeijer, K.; Scott, K.; Xu, T.; Zhuang, L. Anion-Exchange Membranes in Electrochemical Energy Systems. *Energy Environ. Sci.*, **2014**, 7, 3135–3191.

(28) Gu, S.; Wang, J.; Kaspar, R. B.; Fang, Q.; Zhang, B.; Coughlin, E. B.; Yan, Y. Permethyl Cobaltocenium ($Cp^{*}_{2}Co^{+}$) as an Ultra-Stable Cation for Polymer Hydroxide-Exchange Membranes. *Sci. Rep.*, **2015**, 5, 1–11.

(29) Marino, M. G.; Kreuer, K. D. Alkaline Stability of Quaternary Ammonium Cations for Alkaline Fuel Cell Membranes and Ionic Liquids. *ChemSusChem*, **2015**, 8, 513–523.

(30) Noonan, K. J. T.; Hugar, K. M.; Kostalik, H. A.; Lobkovsky, E. B.; Abruña, H. D.; Coates, G. W. Phosphonium-Functionalized Polyethylene: A New Class of Base-Stable Alkaline Anion Exchange Membranes. *J. Am. Chem. Soc.*, **2012**, 134, 18161–18164.

(31) Pham, T. H.; Olsson, J. S.; Jannasch, P. N-Spirocyclic Quaternary Ammonium Ionenes for Anion-Exchange Membranes. *J. Am. Chem. Soc.*, **2017**, 139, 2888–2891.

(32) Zha, Y.; Disabb-Miller, M. L.; Johnson, Z. D.; Hickner, M. A.; Tew, G. N. Metal-Cation-Based Anion Exchange Membranes. *J. Am. Chem. Soc.*, **2012**, 134, 4493–4496.

(33) Thomas, O. D.; Soo, K. J. W. Y.; Peckham, T. J.; Kulkarni, M. P.; Holdcroft, S. A Stable Hydroxide-Conducting Polymer. *J. Am. Chem. Soc.*, **2012**, 134, 10753–10756.

(34) Wright, A. G.; Holdcroft, S. Hydroxide-Stable Ionenes. *ACS Macro Lett.*, **2014**, 3, 444–447.

(35) Wright, A. G.; Fan, J.; Britton, B.; Weissbach, T.; Lee, H. F.; Kitching, E. A.; Peckham, T. J.; Holdcroft, S. Hexamethyl-*p*-terphenyl Poly(benzimidazolium): A Universal Hydroxide-Conducting Polymer for Energy Conversion Devices. *Energy Environ. Sci.*, **2016**, 9, 2130–2142.

(36) Fauchais, P. L.; Heberlein, J. V. R.; Boulos, M. *Thermal Spray Fundamentals: From Powder to Part*, Springer, NY, USA, **2014**, page 23.

(37) Schiller, G.; Henne, R.; Borck, V. Vacuum Plasma Spraying of High-Performance Electrodes for Alkaline Water Electrolysis. *J. Therm. Spray Technol.*, **1995**, 4, 185–194.

(38) Liu, T.; Reißner, R.; Schiller, G.; Ansar, A. Experimental and Numerical Study of the

Effect of Gas-Shrouded Plasma Spraying on Cathode Coating of Alkaline Electrolysis Cells. *J. Therm. Spray Technol.*, **2018**, 27, 35–49.

(39) Ayers, K.; Danilovic, N.; Ouimet, R.; Carmo, M.; Pivovar, B.; Bornstein, M. Perspectives on Low Temperature Electrolysis and Potential for Renewable Hydrogen at Scale. *Annu. Rev. Chem. Biomol. Eng.*, **2019**, 10, 219–239.

(40) Hackemüller, F. J.; Borgardt, E.; Panchenko, O.; Müller, M.; Bram, M. Manufacturing of Large-Scale Titanium-Based Porous Transport Layers for Polymer Electrolyte Membrane Electrolysis by Tape Casting. *Adv. Eng. Mater.*, **2019**, 21, 1801201.

(41) Friedrich, K. A.; Lettenmeier, P.; Ansar, A. S.; Wang, L.; Gago, A. S. Achieving Cost Reduction in PEM Electrolysis by Material Development. *Proceedings in 6th European PEFC & Electrolyser Forum*, **2017**, July, 31–40.

(42) Ansar, A.; Reissner, R.; Aguiar, D.; Liu, T.; Schiller, G. Raney-Nickel Alloy Electrodes for Alkaline Water Electrolysis. *1st International Conference of Electrolysis*, Copenhagen, **2017**.

(43) Ziv, N.; Dekel, D. R. A Practical Method for Measuring the True Hydroxide Conductivity of Anion Exchange Membranes. *Electrochem. commun.*, **2018**, 88, 109–113.

(44) Medway, S. L.; Lucas, C. A.; Kowal, A.; Nichols, R. J.; Johnson, D. In Situ Studies of The Oxidation of Nickel Electrodes in Alkaline Solution. *J. Electroanal. Chem.*, **2006**, 587, 172–181.

(45) Hall, D. S.; Bock, C.; MacDougall, B. R. The Electrochemistry of Metallic Nickel: Oxides, Hydroxides, Hydrides and Alkaline Hydrogen Evolution. *J. Electrochem. Soc.*, **2013**, 160, F235–F243.

(46) Oshchepkov, A. G.; Bonnefont, A.; Saveleva, V. A.; Papaefthimiou, V.; Zafeiratos, S.; Pronkin, S. N.; Parmon, V. N.; Savinova, E. R. Exploring the Influence of the Nickel Oxide Species on the Kinetics of Hydrogen Electrode Reactions in Alkaline Media. *Top. Catal.*, **2016**, 59, 1319–1331

(47) Gorlin, M.; De Araujo, J. F.; Schmies, H.; Bernsmeier, D.; Dresp, S.; Gliech, M.; Jusys, Z.; Chernev, P.; Kraehnert, R.; Dau, H.; Strasser, P. Tracking Catalyst Redox States and Reaction Dynamics in Ni-Fe Oxyhydroxide Oxygen Evolution Reaction Electrocatalysts: The Role of Catalyst Support and Electrolyte pH. *J. Am. Chem. Soc.*, **2017**, 139, 2070–2082.

(48) Yuan, X.; Wang, H.; Sun, J. C.; Zhang, J. AC Impedance Technique in PEM Fuel Cell Diagnosis-A Review. *Int. J. Hydrogen Energy*, **2007**, 32, 4365–4380.

(49) Rozain, C.; Millet, P. Electrochemical Characterization of Polymer Electrolyte Membrane Water Electrolysis Cells. *Electrochim. Acta*, **2014**, 131, 160–167.

(50) Miousse, D.; Lasia, A.; Borck, V. Hydrogen Evolution Reaction on Ni-Al-Mo and Ni-Al Electrodes Prepared by Low Pressure Plasma Spraying. *J. Appl. Electrochem.*, **1995**, 25, 592–602.

(51) Danilovic, N.; Subbaraman, R.; Strmcnik, D.; Stamenkovic, V. R.; Markovic, N. M. Electrocatalysis of the HER in Acid and Alkaline Media. *J. Serbian Chem. Soc.*, **2013**, 78, 2007–2015.

(52) Lützenkirchen-Hecht, D.; Frahm, R. Corrosion of Mo in KOH: Time Resolved XAFS Investigations. *J. Phys. Chem. B*, **2001**, 105, 9988–9993.

(53) Bowen, J. R.; Bentzen, J. J.; Stanley, J. P.; Zhang, W. RES Hydrogen: Efficient Pressurised Alkaline Electrolysers. *EU RESelyser Project final report*. **2015**.

(54) Ip, S. W.; Sridhar, R.; Toguri, J. M.; Stephenson, T. F.; Warner, A. E. M. Wettability of Nickel Coated Graphite by Aluminum. *Mater. Sci. Eng. A*, **1998**, 244, 31–38.

TOC Graphic:

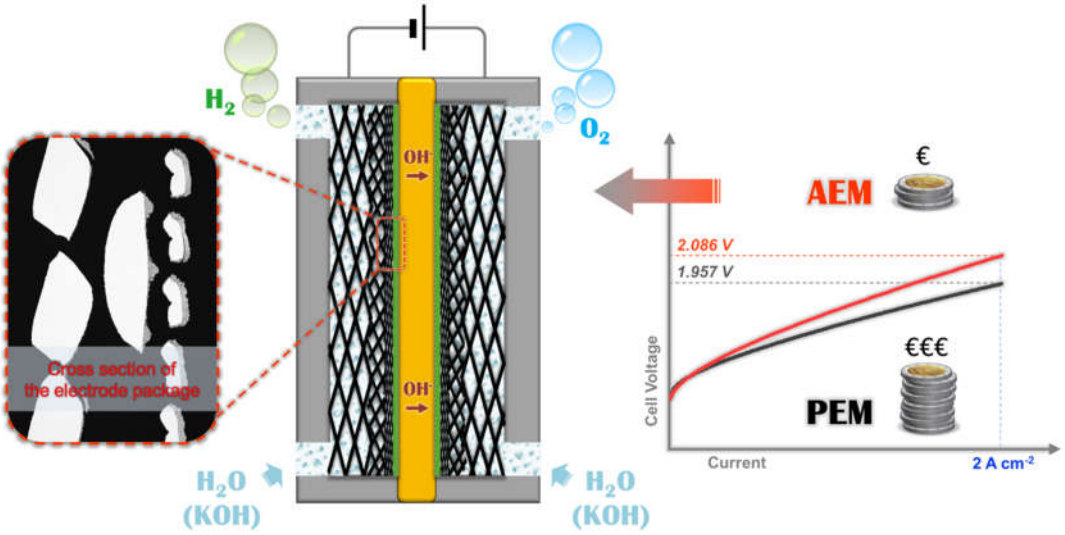
H2
O2
OH-
OH-
Cross section of the electrode package
H2O (KOH)
H2O (KOH)
AEM
€
2.086 V
1.957 V
Cell Voltage
€€€
PEM
Current
2 A cm-2